Self-organized formation of regular nanostripes on vicinal surfaces

Yan-Mei Yu and Bang-Gui Liu
Institute of Physics and Center of Condensed Matter Physics, Chinese Academy of Science, P. O. Box 603, 100080 Beijing, People's Republic of China

(Received 7 June 2004; revised manuscript received 9 September 2004; published 12 November 2004)

We explore the mechanism of self-organized formation of regular arrays of nanostripes on vicinal surfaces by using a phase-field model. Epitaxial growth during deposition usually results in both nanostripes and islands on terraces of a vicinal substrate. Postdeposition annealing at elevated temperatures induces growth of the nanostripes but makes the islands shrink. It is a ripening process of the mixed system of the nanostripes and the islands, being dependent upon the temperature and strain. It is accompanied by a transition from the diffusion-limited regime to the detachment-limited regime induced by the strain at high temperatures. This ripening makes the islands diminish and on the other hand makes the nanostripes smoother. As a result, the islands disappear completely and the regular arrays of nanostripes are formed on the vicinal substrate. This theory can explain the self-organized formation of nanostripes and nanowires on vicinal surfaces, such as the intriguing regular arrays of Fe nanostripes on the vicinal W surfaces.

DOI: 10.1103/PhysRevB.70.205414 PACS number(s): 81.15.Aa, 68.35.Fx, 68.35.Ct

I. INTRODUCTION

Regular arrays of nanostripes of the 3*d* metals such as Fe, Co, and Ni grown on vicinal surfaces of W and Mo are interesting magnetic nanostructures for potential applications.[1–5] The formation of the regular arrays of nanostripes originates from dominance of the step-flow growth that results from the direct capture of adatoms at the steps over the nucleation and growth of islands on the terraces of the vicinal surfaces. If epitaxial growth proceeds in the step-flow mode, which can be realized at high temperatures or with low deposition fluxes, the regular arrays of nanostripes can be formed directly in terms of the periodic structure of the vicinal surfaces. This regime can be described by one-dimensional models, being similar to the step-flow growth on flat substrates, which has been studied by Monte Carlo simulations[6] and numerical solutions of the reaction-diffusion equations.[7]

However, nucleation and growth of islands in addition to nanostripes on a vicinal substrate is inevitable under usual conditions. This leads to a hybrid configuration of nanostripes bound to the substrate steps and islands situated on the terraces. However, the mixed structure can reorder into regular arrays of nanostripes by annealing at elevated temperatures with the flux turned off, i.e., postdeposition annealing.[1] How these regular arrays of nanostripes form is a fascinating but open question, which is important, without a doubt, for preparation of the magnetic nanostripes as well as nanowires on vicinal surfaces. It is known that postdeposition annealing leads to relaxation towards equilibrium. The previously published work on relaxation of nanostructures on surfaces focused on an isolated island or an ensemble of islands on a whole large terrace,[8–11] which undergoes the well-known Oswald ripening.

In this paper, we simulate the self-organized formation of regular nanostripes grown on vicinal surfaces during postdeposition annealing. We shall use a phase-field model,[12–15] which can provide fine images for visualizing the epitaxial morphology together with the distribution of the adatom concentration at reasonable scales of time and space. Atomic detachment, as an element of a reversible growth process, also is included in the phase-field simulations. The phase-field simulated results show that the epitaxial growth at the low temperature leads to a hybrid configuration of nanostripes and islands that are unstable under relaxation conditions during a ripening induced by postdeposition annealing at elevated temperatures. A transition from the diffusion-limited regime into the detachment-limited regime is induced by the strain during ripening. The ripening induces growth of the nanostripes at the expense of the islands, causing the islands to vanish but smoothening the fluctuated nanostripes. The ripening finally leads to the formation of regular arrays of nanostripes. This theory can be used to explain the formation of experimental nanostripes on vicinal surfaces.

The phase-field model for epitaxial growth on vicinal surfaces is presented in the next section. In Sec. III we present the phase-field simulated results. In Sec. IV, we discuss the mechanism of the self-organized formation of regular nanostripes. Finally, we conclude with a summary in Sec. V.

II. PHASE-FIELD MODEL OF EPITAXIAL GROWTH ON VICINAL SURFACES

In this scheme, by defining a continuum variable Φ of value 0, 1, 2, 3…, *n*, which describes sequentially the bottom terrace, the first terrace, the second terrace, the third terrace,…, and the *n*th terrace, we can construct a staircase substrate, each of whose steps is assumed to be of one atomic layer height. Epitaxial growth on the substrate is described by a local increase of the value of Φ, indicating the formation of new atomic layers. The sharp steps between different atomic layers in atomic models are replaced by spatial transition zones, across which Φ varies smoothly from one integer to another. After being deposited on terraces, adatoms diffuse laterally with a rate *D*, producing a continuum field of the local density of adatoms. We let $D=a^2\nu\exp(-E_d/k_BT)$, where *a* is the lattice constant of the physical substrate,

ν is the attempt frequency, E_d is the energy barrier of diffusion, k_B is the Boltzmann constant, and T is the temperature. The influx of adatoms makes the local density of adatoms u much larger than the equilibrium concentration of adatoms at the substrate, which drives the evolution of Φ.

Our starting point is the free energy functional

$$H = \int dV\left[\tfrac{1}{2}W^2(\nabla\Phi)^2 + f(\Phi,u)\right], \tag{1}$$

where the energy density f is formulated phenomenologically as

$$f(\Phi,u) = -\frac{1}{\pi}\cos(2\pi\Phi) + \lambda u\left[\frac{1}{\pi}\sin(2\pi\Phi) - 2\Phi\right], \tag{2}$$

in order to make H reach degenerate minimums at $\Phi = 1,2,3\ldots,n$. This implies that the system is metastable when $\Phi = 1,2,3\ldots,n$, and deposited adotoms continually make the system unstable, forming new atomic layers on original terraces.

A variational formulation of the phase field model that guarantees that H decreases monotonically in time ($dH/dt \leqslant 0$) is

$$\frac{\partial\Phi}{\partial t} = -\frac{1}{\tau}\frac{\delta H}{\delta\Phi} = \frac{1}{\tau}(W^2\nabla^2\Phi - 2\sin 2\pi\Phi) - 2(\cos 2\pi\Phi - 1)\lambda u + \lambda_n u^2, \tag{3}$$

where the model parameter W represents the width of the phase-field transition zone, τ is the characteristic time of attachment of adatoms at steps, and λ is a dimensionless coupling constant.

By using the *thin-interface-limit analysis*,[12] the model parameters are related to the characteristic parameters of the system according to the following equations:

$$\lambda = \frac{a_1 W}{\pi d_0}, \tag{4}$$

$$\tau = \frac{a_1 a_2 W^3}{D d_0}, \tag{5}$$

where d_0 is the capillarity length, which evaluates the deviation of the local equilibrium concentration of adatoms at a curved step from that at a straight step. We know

$$d_0 = \frac{a^2 c_{\mathrm{eq}}\gamma}{k_B T}, \tag{6}$$

where c_{eq} is the equilibrium concentration at a straight step and γ is the step stiffness. The numerical constants a_1 and a_2 are determined by the form of the free-energy density and are evaluated to be 0.36 and 0.51, respectively, in terms of the thin-interface-limit analysis.

According to the principle of mass conservation, the diffusion equation governing u is given by

$$\frac{\partial u}{\partial t} = \nabla\cdot D\nabla u - \frac{\partial\Phi}{\partial t} + \delta(r-r')\delta(t-t'), \tag{7}$$

where the first term on the right side of Eq. (7) represents the lateral diffusion. We modify D in the phase-field transition zone to take into account the effect of the Schwoebel barrier E_s on the downward motion of adatoms. The terrace-climbing motion of adatoms also is inhibited. The term $\partial\Phi/\partial t$ describes consumption of adatoms resulting from the evolution of Φ. The third term on the right side of Eq. (7) represents the random deposition of adatoms. The random influx of adatoms is reflected by the term $\lambda_n u^2$ in the phase-field Eq. (3), which triggers spontaneous nucleation of islands. The exponent 2 comes from the assumption that the critical size of an island is 1. Here we introduce a parameter λ_n to describe the nucleation rate of islands.

The epitaxial growth may be reversible, especially at high temperatures. The "dead" adatoms belonging to an island or a nanostripe may detach from the edge of the island or the nanostripe. Supposing here that misfit strain enhances the detachment rate, we obtain $\exp[-(a_i E_i - E_e)/k_B T]$ as the detachment probability, where E_i is the atomic binding energy, E_e is the elastic energy, and a_i is an artificial parameter defined for the phase-field model, as a coarse-grained continuum model, to replace the nearest atom number in lattice models. For every iteration we check if the detachment of adatoms happens or not, according to the detachment probability at all spatial grids at the edges of the islands and the nanostripes. If the detachment happens, we shall reduce the value of Φ by $1/(\Delta x)^2$. Correspondingly, we augment the adatom concentration by $1/(\Delta x)^2$ at the nearest grid node of the lowest Φ, where Δx is the spacing of the grids.

The misfit strain changes stress of the islands and that of the nanostripes in different ways, therefore we formulate the strain energy of the islands and that of the nanostripes in different ways. The misfit strain induces a force monopole on both edges of each nanostripe, forming in effect a stress domain structure. The elastic energy per unit area of the nanostripe in the stress domain structure is formulated as[16,17]

$$E_{\mathrm{stripe}} = \frac{2C}{L}\ln\left(\frac{L}{2\pi a}\sin\frac{\pi w}{L}\right), \tag{8}$$

where w is the nanostripe width, L is the terrace width, and C is given by

$$C = \frac{4}{\pi}\frac{1+\sigma}{1-\sigma}E\epsilon^2, \tag{9}$$

where σ is the poisson ratio, E is the Young modulus, and ϵ is the misfit. For an island, the force monopole operates along the island's perimeter, and the elastic energy per unit area is formulated as[18,19]

$$E_{\mathrm{island}} = \frac{2C}{\pi d}\ln\frac{d}{2a}, \tag{10}$$

where d is the diameter of the island. Two simplifications are made to derive Eqs. (8)–(10): (i) Any interaction between two islands or between an island and a nanostripe is neglected; (ii) Undulation of the advancing free edge of the

nanostripes may change the stress domain structure and the elastic strain energy of the nanostripe,[20] a phenomenon which is neglected here.

Equations (3) and (7) are discretized in a square domain of size $l\Delta x$, where l is the number of the spatial grid nodes, by using the second-order finite difference method on uniform Cartesian grids, and by using the first-order finite difference approximation in the time domain. In addition to the restriction that $\Delta t < (\Delta x)^2(5D)^{-1}$, the value of time step Δt is also kept low enough to ensure the conservation of mass. The periodic boundary condition is used in all directions.

III. PHASE-FIELD RESULTS OF FORMATION OF NANOSTRIPES

In the phase-field simulations, we measure length in units of a, which indicates $a=1$ in the relative expression. We take W as an input parameter, then determine λ and τ according to Eqs. (4) and (5) with the systematic parameters determined. There is not yet exact experimental or calculated data accessible for the atomic kinetic on W(110). Here, we choose $E_d = 0.53$ eV, an intermediate value between the diffusion barrier for the homoepitaxy system of Fe[21] and that for the homoepitaxy system of W;[22,23] $E_i = 0.50$ eV, being the same as the bond energy of an Fe—Fe atom pair in the Fe/Fe(100) system;[21] $E_s = 0.06$ eV, an intermediate Schwoebel barrier for metal systems;[24] $\nu = 10^{12}$, a usual value for metal systems. In addition, we choose $E = 2.0 \times 10^{12}$ dyn/cm^2 and $\sigma = 0.28$ in the calculation of the elastic energy, referring to the elastic mechanical property of Fe.[25] The terrace width of the vicinal surface is chosen to be the experimental value $30a$.[1]

Furthermore, we adjust d_0 and λ_n to match simulated results to the experimental images of Fe/W(110). We first simulate the epitaxial growth on the vicinal substrate at $T = 300$ K and achieve the simulated images that resemble the scanning tunneling microscopy images[1] of Fe on W(110) vicinal surface at the same temperature. Here d_0 is taken as 1.5×10^{-5}, which is consistent with the value evaluated according to Eq. (6) with $c_{eq} \sim \exp(a_i E_i)$ where $a_i = 1-2$, and $\gamma = 2.55$ J m^{-2}, the value of the surface energy of Fe.[26] The agreement of the simulated images with the experimental ones indicates that the values of our parameters are reasonable, which guarantees the reliability of the following qualitative simulations.

Neglecting the variation of C_{eq} in the temperature range of 300–600 K, we derive $d_0 \sim T^{-2}$ from Eq. (6) with $\gamma \sim T^{-1}$. Then we choose values of d_0 at the other temperatures according to the value of d_0 at $T = 300$ K. The nucleation of islands is neglected in the simulations for the postdeposition annealing at high temperatures. The dependence of phase-field simulated results on the model parameters as well as the simulation parameters has been discussed in Ref. 14. The reasonable values of these parameters, as shown in Table I, allow us to simulate the epitaxial growth qualitatively.

Figure 1 shows the simulated images of the epitaxial growth on the vicinal surface at $T = 300$ K. It is clear that the epitaxial growth starts with both the nucleation of the islands and the step-flow growth at the substrate steps, but the former is dominant over the latter. With the coverage increasing, the islands grow, coalesce, and are connected to the decoration at the substrate steps, forming a connected structure of one atom height; and then new islands start to nucleate on the connected structure. Subtracting the substrate from the morphology in Fig. 1, we obtain the distribution of the atomic-layer thickness on the vicinal substrate with coverage larger than one monolayer (ML), as shown in Fig. 2. This figure shows that channels of the connected structure shrink and finally disappear as the coverage increases further, and in contrast many complete nanostripes are formed. The nanostripes are stacked, forming double layer (DL) stripes, which extend along the substrate steps. However, the grown second-layer islands disturb the DL nanostripes, which leads to a mixed structure of nanostripes and islands.

TABLE I. The parameters used in the phase-field simulations: temperature T (K), diffusion rate D (units of a^2/s), the three model parameters W (units of a), λ and τ (s), the two simulation parameters Δx (units of a) and Δt (s).

T	D	W	λ	τ	Δx	Δt
300	8.4×10^3	4	7.8×10^4	77	2	10^{-4}
400	2.1×10^5	4	8.7×10^4	3.0	2	10^{-6}
500	4.5×10^6	4	1.8×10^5	0.3	2	5×10^{-7}
600	3.5×10^7	4	2.0×10^5	0.045	2	1×10^{-7}

Then, we focus on the time evolution of the epitaxial overlayer as shown in Fig. 1(d) after the flux is turned off. The simulations are designed for two cases. For one case no strain is taken into account, and for the other case the 10% misfit strain (a value for the system of Fe/W) is included

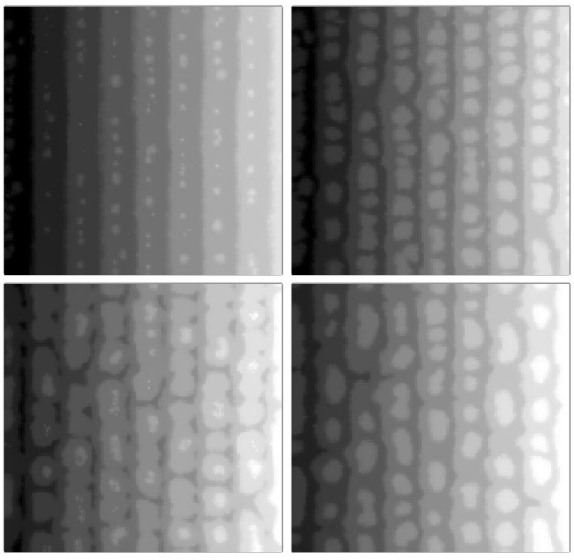

FIG. 1. The simulated images, on $250\times250a^2$ (a is the lattice constant of the substrate), of epitaxial morphology on the vicinal substrate at $T = 300$ K for the different coverages of (a) 0.24, (b) 0.69, (c) 1.21, and (d) 1.66 ML. The white arrow points to the nanostripe, and the black the island. From right to left is the downward direction of the vicinal substrate. The model and simulation parameters are given in Table I.

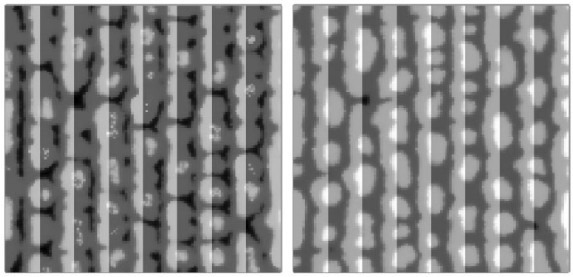

FIG. 2. The atomic-layer thickness distribution on the vicinal substrate of $250\times250a^2$, with coverages of (a) 1.21, and (b) 1.66 ML. The change from dark to light color represents in sequence the substrate, the first atomic layer (AL), the second AL, and the third AL. The white arrow points to the nanostripe, and the black the island. All the parameters are the same as in Table I.

into the simulations. The two types of simulations both are preformed at $T=400$, 500, and 600 K, respectively.

Figure 3 presents simulated images of the epitaxial overlayer during postdeposition annealing at $T=500$ K in the presence of the misfit strain. The distribution of adatom concentration on the vicinal substrate is correspondingly shown in Fig. 4. Figure 3(a) shows that the epitaxial morphology on the vicinal substrate still do not appear to change at the initial stage of annealing. The convex steps, which were produced by the coalescence of the islands in the epitaxial growth at $T=300$ K, remain distributed along the free edges of the nanostripes. At these convex steps, the adatom concentration meets the local minimum, forming local sinks for adatom concentration, as shown in Fig. 4(a).

Figure 3(b) shows that during annealing, the islands on the terraces start to decay while the nanostripes expand laterally with their free edges advancing forward (leftward is

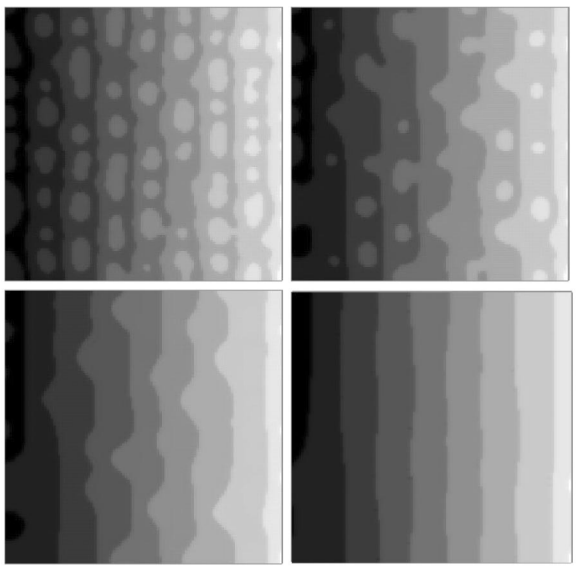

FIG. 3. The simulated ripening images, on $250\times250a^2$, of an epitaxial overlayer during postdeposition annealing at $T=500$ K at (a) $t=2$ s, (b) $t=40$ s, (c) $t=100$ s, and (d) $t=600$ s. From right to left is the downward direction of the vicinal substrate. All the parameters are the same as in Table I.

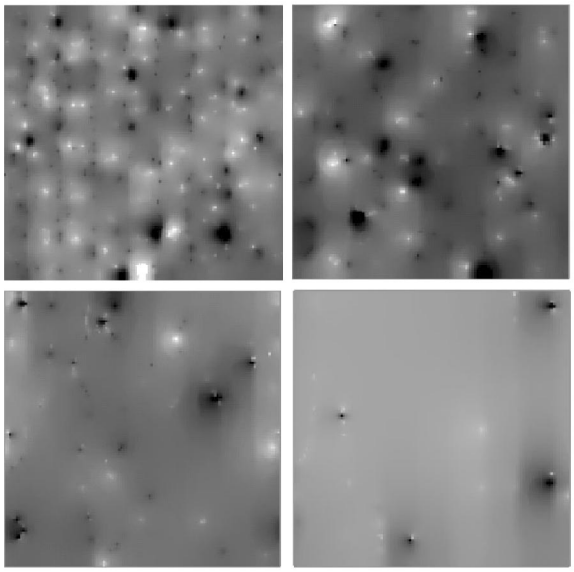

FIG. 4. The adatom concentration on the vicinal substrate of $250\times250a^2$ corresponding to Fig. 3 at (a) $t=2$ s, (b) $t=40$ s, (c) $t=100$ s, and (d) $t=600$ s. All the parameters are the same as in Table I.

the growth direction). Some islands coalesce into the nanostripes, which happens in the areas nearest to the convex steps. Coalescence of the islands and the nanostripes forms the lateral mounds at the free edges of the nanostripes. The residual islands on terraces, which are a little far from the convex edges of the nanostripes, become isolated and continue decaying. Figure 4(b) shows that the decaying islands become sources of the adatom concentration in contrast to the sinks for adatom concentration at the convex edges of the nanostripes.

Figure 3(c) shows that the islands continue to diminish until there are only the nanostripes left on the vicinal substrate as the annealing continues. These nanostripes have the alternating ML and DL thickness, as shown in Fig. 5(a). The mounds produced by the coalescence of the islands and the nanostripes cause the fluctuation of the free edges of the nanostripes, therefore the spacing of the nanostripes is not uniform. Figure 4(c) shows that the adatom concentration has become uniform in most areas on the vicinal substrate

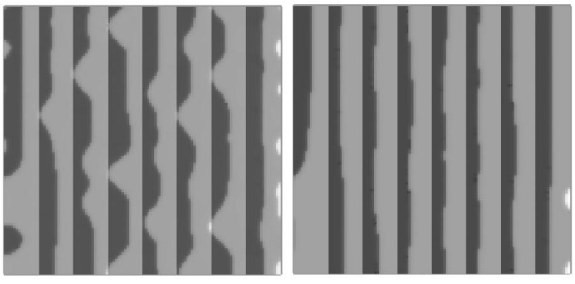

FIG. 5. The simulated images on $250\times250a^2$ of the array of double layer nanostripes during postdeposition annealing at (a) $t=100$ s and (b) $t=600$ s. The dark-gray and the light-gray represent the first AL and the second AL, respectively. All the parameters are the same as in Table I.

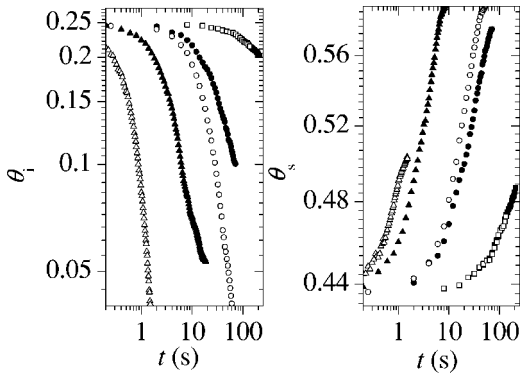

FIG. 6. The varying coverage of the islands (left panel) and of the nanostripes (right panel) during the postdeposition annealing at $T=400$ K (square), $T=500$ K (circle), $T=600$ K (triangle) for the cases that the strain is absent (solid points) and that the strain is present(open points). All the parameters are the same as in Table I.

although some sinks still exist near the roots of the mounds at this stage of the annealing. With the annealing going further, the mounds decay and the free edges of the nanostripes become smoother and smoother. Finally the regular arrays of nanostripes with a uniform periodic spacing are formed on the vicinal substrate, as shown in Figs. 3(d) and 5(b). The distribution of the adatom concentration becomes more uniform on the vicinal substrate, as shown in Fig. 4(d).

The nanostripes and the islands evolve in similar ways at the other temperatures with or without the strain. Figure 6 shows the logarithmic plots of the coverage of the islands θ_i versus the annealing time t and the coverage of the DL nanostripes θ_s vs t. The left panel is for θ_i, and the right panel is for θ_s. This figure shows that θ_i decreases with t but θ_s increase with t, indicating the growth of the nanostripes at the expense of the islands for all cases.

Furthermore, the parabolic parts of the plots of θ_i vs t and θ_s vs t indicate that the rate of change of θ_i and that of θ_s both increase with t at the first stage. Then the rate of change of θ_i as well as that of θ_s approaches a steady value, which is indicated by the linear parts of these plots, except that at $T=400$ K θ_i and θ_s vary too slowly to approach a steady rate of change in the limited time window of our simulations. The higher the temperature, the faster θ_i and θ_s vary to meet the steady rate. As a whole, the high temperature enhances the variation of θ_i and θ_s. For the different temperatures, the plots of θ_i vs t indicate the same power-law exponent according to their linear parts. The exponent is about 0.6 for the case in which the misfit strain is absent. In comparison, the exponent is improved to 1.16 at $T=500$ K and $T=600$ K with the presence of the misfit strain, indicating a larger rate. At $T=400$ K the misfit strain causes no evident effect on the exponent. The power-law exponent for θ_s remains about 0.13 at the different temperatures with or without the strain.

IV. MECHANISM OF FORMING REGULAR NANOSTRIPES

The epitaxial growth on the vicinal surface at $T=300$ K produces a hybrid structure of the nanostripes and the islands. During the postdeposition annealing, further relaxation of the hybrid structure is driven by the tendency of minimizing the total step energy. Related to the local curvature of the step, the relaxation proceeds with the Gibbs-Thomson effect,[27] i.e., the features with the lowest curvature have the largest growth motivation. Therefore, the growth motivation is largest along the convex edges of the nanostripes, where the local curvature is smallest, even being negative sometimes, with the growth direction of the nanostripe being positive. Consequently, the cost for adatoms is largest here, leading to the local minimum of the adatom concentration, i.e., the sink for adatom concentration. In contrast, the islands on the terraces and the lateral mounds at the edges of the nanostripes, which are encircled by the concave steps, have a large step curvature locally and exhibit low growth motivation. Hence, the adatom concentration is high near these features. Thus, some net mass currents arise, from the islands on the terraces to the nanostripes, and the other currents arise similarly, from the lateral mounds at the edges of the nanostripes to their bilateral valleys. These mass currents are maintained by the sinks for adatom concentration at the convex steps during the annealing.

Along with the adatom currents from the islands to the nanostripes, the islands adjacent to the convex edges of the nanostripes coalesce with the nanostripes, and the other islands a little far from these convex steps still decay persistently. Accordingly, the nanostripes grow forward with the adatoms attaching and the islands coalescing into them. Furthermore, the adatom currents from the lateral mounds at the edges of the nanostripes to their bilateral valleys smoothen the nanostripes with the mounds decaying gradually. Therefore, mediated by the adatom currents among the features on the vicinal substrate, the relaxation of the original mixed system of the nanostripes and the islands undergoes a ripening wherein the nanostripes grow at the expense of the islands to lower the total step energy. The ripening makes the islands diminish and on the other hand smoothens the nanostripes, eventually leading to the self-organized formation of the regular arrays of nanostripes, a structure of better stability in energy.

The ripening kinetic is reflected by the decrease of the islands, which controls the formation of the regular arrays of nanostripes. Consider a single island. There may be two adatom currents responsible for the decay of the island. One adatom current is induced by the adatom concentration gradient near the island. If the misfit strain is present, an extra adatom current is induced by the enriched atomic detachment from the edge of the island, which is independent of the adatom concentration nearby. We can expressed the declining rate of the island radius, r, induced by the two adatom currents as the following equation:[9]

$$r\frac{dr}{dt} = -D'\frac{1}{r} - D'_d, \tag{11}$$

where the two terms on the right of Eq. (11) represent sequentially the diffusion adatom current induced by the adatom concentration gradient and the adatom current induced by the atomic detachment. The parameters D' and D'_d are

related to the diffusion rate and the detachment rate, respectively.

Equation (11) indicates that the decaying rate of an island is enhanced by the high temperature and the strain by increasing D' and D'_d, respectively, which agrees with the simulated results illustrated in Fig. 6. As a whole, the high temperature and the strain enhance the ripening, and therefore accelerate the formation of the regular arrays of nanostripes during the postdeposition annealing.

When the misfit strain is absent, the declining rate of r is determined by the diffusion of adatoms. By integrating Eq. (11) according to the diffusing adatom current, we obtain

$$A \propto D'(t_0 - t)^{2/3}, \tag{12}$$

where A is the island area and t_0 is the time when r decreases to be zero. From Eq. (12), we deduce that the power-law exponent of A vs t is $2/3$, being consistent with the steady-state value of θ_i vs t obtained without the misfit strain, which indicates that the ripening of the hybrid structure is diffusion-limited for the case the misfit strain is absent.

As for the case in which the atomic detachment becomes dominant for the decay of the island, we obtain

$$A \propto D'_d(t_0 - t) \tag{13}$$

by integrating Eq. (11) in terms of the detachment current of adatoms. Equation (13) indicates that the power-law exponent of A vs t is 1, consistent with the steady-state value of θ_i vs t obtained for the cases the misfit strain is present at $T=500$ K and $T=600$ K. This means that at $T=500$ and 600 K the elastic strain energy enhances the atomic detachment so greatly that the ripening of the hybrid structure is driven into the detachment-limited regime, where the ripening rate is larger than that in the diffusion-limited regime. At $T=400$ K, the atomic detachment is not activated by the elastic strain energy, therefore the ripening remains diffusion-limited.

Moreover, the features on the vicinal substrate have different elastic strain energy. Figure 7 gives the elastic strain energy, calculated according to Eqs. (8)–(10) for the island and the nanostripe on a vicinal substrate. This figure indicates that when the terrace width of the vicinal substrate is between $20a$ and $40a$, a reasonable numerical range for inhibiting dislocations in epitaxial structures,[1] almost for all sizes, the elastic strain energy of the islands is larger than that of the nanostripes. This means that there may be more atomic detachment, enhanced by the larger strain energy, at the edges of the islands, which accelerates further the decay of the islands and then leads to the formation of the regular arrays of nanostripes.

The elastic strain energy may be changed by the interaction among the islands and nanostripes as well as undulation of the nanostripes. However, in any case, the adatom current induced by the enriched atomic detachment always complies with the directional mass currents induced by the sinks of adatom concentration at the convex steps, which ensures the formation of the regular arrays of nanostripes on the vicinal surface.

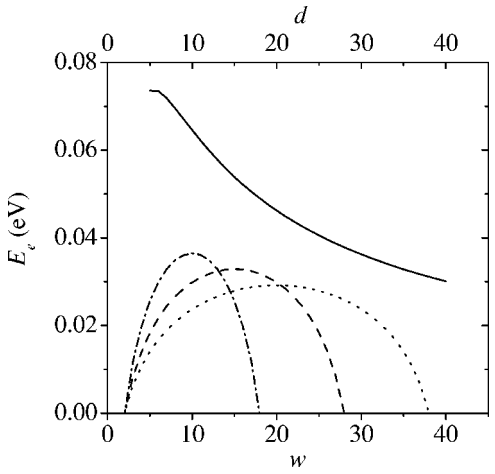

FIG. 7. The elastic strain energy per atom of the islands (the solid line) and of the nanostripes (the broken line) on the vicinal surface with the terrace width of 20, 30, and 40 a (from the left to right).

V. CONCLUSION

In summary, we have explored the mechanism of the self-organized formation of regular arrays of nanostripes on vicinal surfaces through the phase-field simulations. The nanostripes and the islands are formed simultaneously on the vicinal substrate in the epitaxial growth at the room temperature, but they both tend to ripen during the postdeposition annealing at the elevated temperatures. The ripening, accelerated by the strain, on one hand drives the islands to vanish, and on the other hand makes the nanostripes grow wider and smoother. There is a transition, induced by the strain at the high temperatures, from the diffusion-limited regime to the detachment-limited regime. As a result of the ripening, the regular arrays of nanostripes are formed on the vicinal substrate in a self-organized way. The phase-field theory can be used to describe the formation of regular arrays of nanostripes and nanowires on vicinal surfaces, such as the well-known Fe nanostripes on W crystal surfaces.

ACKNOWLEDGMENTS

This work is supported by Chinese Department of Science and Technology under the National Basic Research Projects (No. G1999064509) and by the Natural Science Foundation of China.

[1] M. Bode, R. Pascal, M. Dreyer, and R. Wiesendanger, Phys. Rev. B **54**, R8385 (1996); O. Pietzsch, A. Kubetzka, M. Bode, and R. Wiesendanger, Phys. Rev. Lett. **84**, 5212 (2000); Science **292**, 2053 (2001); M. Bode, S. Heinze, A. Kubetzka, O. Pietzsch, X. Nie, G. Bihlmayer, S. Blugel, and R. Wiesendanger, Phys. Rev. Lett. **89**, 237205 (2002); M. Bode, O. Pietzsch, A. Kubetzka, and R. Wiesendanger, *ibid.* **92**, 067201 (2004).

[2] H. J. Elmers, J. Hauschild, H. Hoche, U. Gradmann, H. Bethge, D. Heuer, and U. Kohler, Phys. Rev. Lett. **73**, 898 (1994); J. Hauschild, U. Gradmann, and H. J. Elmers, Appl. Phys. Lett. **72**, 3211 (1998); H. J. Elmers, J. Hauschild, and U. Gradmann, Phys. Rev. B **59**, 3688 (1999).

[3] S. Murphy, G. Mariotto, N. Berdunov, and I. V. Shvets, Phys. Rev. B **68**, 165419 (2003).

[4] D. Reuter, G. Gerth, and J. Kirschner, Phys. Rev. B **57**, 2520 (1998).

[5] M. Mura, P. Ruggerone, and V. Fiorentini, Phys. Rev. B **67**, 153406 (2003).

[6] J. P. G. Taylor, K. J. Hugill, D. D. Vvedensky, and A. MacKinnon, Phys. Rev. Lett. **67**, 2359 (1991).

[7] C. Ratsch, M. D. Nelson, and A. Zangwill, Phys. Rev. B **50**, 14 489 (1994).

[8] W. Theis, N. C. Bartelt, and R. M. Tromp, Phys. Rev. Lett. **75**, 3328 (1995).

[9] J. G. McLean, B. Krishnamachari, D. R. Peale, E. Chason, J. P. Sethna, and B. H. Cooper, Phys. Rev. B **55**, 1811 (1997).

[10] K. Morgenstern, G. Rosenfeld, and G. Comsa, Phys. Rev. Lett. **76**, 2113 (1996); K. Morgenstern, G. Rosenfeld, E. Lagsgaard, F. Besenbacher, and G. Comsa, *ibid.* **80**, 556 (1998).

[11] D. M. Tarr and P. A. Mulheran, Phys. Rev. E **68**, 020602 (2003).

[12] A. Karma and W. J. Rappel, Phys. Rev. Lett. **77**, 4050 (1996); A. Karma and M. Plapp, *ibid.* **81**, 4444 (1998).

[13] F. Liu and H. Metiu, Phys. Rev. E **49**, 2601 (1994).

[14] Y. M. Yu and B. G. Liu, Phys. Rev. E **69**, 021601 (2004).

[15] O. Pierre-Louis, Phys. Rev. E **68**, 021604 (2003).

[16] O. L. Alerhand, D. Vanderbilt, R. D. Meade, and J. D. Joannopoulos, Phys. Rev. Lett. **61**, 1973 (1988).

[17] A. Li, F. Liu, D. Y. Petrovykh, J. L. Lin, J. Viernow, F. J. Himpsel, and M. G. Lagally, Phys. Rev. Lett. **85**, 5380 (2000).

[18] C. Duport, C. Priester, and J. Villain, in *Morphological Organization in Epitaxial Growth and Removal*, edited by Z. Zhang and M. G. Lagally (World Scientific, Singapore, 1998), pp. 73–93.

[19] F. Liu, A. H. Li, and M. G. Lagally, Phys. Rev. Lett. **87**, 126103 (2001).

[20] J. Tersoff and E. Pehlke, Phys. Rev. Lett. **68**, 816 (1992).

[21] J. A. Stroscio and D. T. Pierce, Phys. Rev. B **49**, 8522 (1994).

[22] G. Ehrlich, Surf. Sci. **331/333**, 865 (1995).

[23] G. Antczak and G. Ehrlich, Phys. Rev. Lett. **92**, 166105 (2001).

[24] J. W. Evans and M. C. Bartelt, in *Morphological Organization in Epitaxial Growth and Removal*, edited by Z. Zhang and M. G. Lagally (World Scientific, 1998), p. 50.

[25] Hans P. R. Frederikse, in *A Physicist's Desk Reference: The Second Edition of Physics Vade Mecum*, edited by H. L. Anderson, B. K. Anderson, and G. C. Marshall (American Institute of Physics, Woodbury, NY, 1989), p. 312.

[26] J. Malzbender, M. Przybylski, J. Giergiel, and J. Kirschner, Surf. Sci. **414**, 187 (1998).

[27] I. M. Lifshitz and V. V. Slyozov, Sov. Phys. JETP **8**, 331 (1959); J. Phys. Chem. Solids **19**, 35 (1961).